

## The Effect of Concentration on PES/NMP System on Flat Sheet Membrane Fabrication and its Performance for CO<sub>2</sub> Gas Separation

Mohamad Alif Adnan, Muhd Izzudin Fikry Zainuddin and Abdul Latif Ahmad\*

School of Chemical Engineering, Universiti Sains Malaysia, Engineering Campus,  
14300 Nibong Tebal, Pulau Pinang, Malaysia.

\*Corresponding author: [chlatif@usm.my](mailto:chlatif@usm.my)

Published online: 25 August 2023

To cite this article: Adnan, M. A. et al. (2023). The effect of concentration on PES/NMP system on flat sheet membrane fabrication and its performance for CO<sub>2</sub> gas separation. *J. Phys. Sci.*, 34(2), 101–114. <https://doi.org/10.21315/jps2023.34.2.8>

To link to this article: <https://doi.org/10.21315/jps2023.34.2.8>

**ABSTRACT:** Carbon dioxide (CO<sub>2</sub>) capture utilising membrane technology have become the interest of research due to its low carbon footprint, feasible fabrication process and scalability in its operation. In this study, anisotropic polyethersulfone (PES) membrane was fabricated at various concentration ranging from 20 wt% to 35 wt% without the use of any additives. This study revealed that the finger-like structure disappeared with increased polymer dope concentration which was associated with increased viscosity of the dope solution. Moreover, the surface porosity of the membrane also virtually reduced with increased PES concentration as observed with the SEM images. The pure gas permeation test was also consistent with the observed morphology of the membrane. Membrane made with 20 wt% of PES dope solution exhibits the highest gas permeance which was 154.9 GPU at 2 bar while the CO<sub>2</sub>/nitrogen (N<sub>2</sub>) and CO<sub>2</sub>/methane (CH<sub>4</sub>) ideal selectivity was close to that of Knudsen's selectivity value. With increased PES concentration, the CO<sub>2</sub> gas permeance reduced drastically accompanied by enhancement on the CO<sub>2</sub>/N<sub>2</sub> and CO<sub>2</sub>/CH<sub>4</sub> ideal selectivity. The critical concentration of PES dope solution obtained by plotting the PES dope concentration against viscosity was 29.4 wt%. With critical concentration of the dope solution, the CO<sub>2</sub> permeance was recorded to be 8.1 GPU while the CO<sub>2</sub>/N<sub>2</sub> and CO<sub>2</sub>/CH<sub>4</sub> ideal selectivity were recorded to be 2.13 and 1.48, respectively at the pressure of 2 bar.

**Keywords:** gas separation, CO<sub>2</sub> capture, polymeric membrane, climate change and phase inversion

## 1. INTRODUCTION

Carbon dioxide (CO<sub>2</sub>) is one of the anthropogenic gases emitted to the atmosphere yearly which contributes to global warming. Over the course of the year, CO<sub>2</sub> concentration is now 50% higher compared to the preindustrial level. Various means have been sought to reduce CO<sub>2</sub> emission to mitigate the climate change issue.<sup>1,2</sup> In gas separation field, membrane is one of the economically viable options available due to its simplicity of the operating process, low energy consumption and small carbon footprint.<sup>3</sup> Although isotropic dense membrane exhibit high gas selectivity, the gas flux is due to the resistance imposed by the dense structure of the membrane. Minimising the dense layer is crucial in order to achieve high gas flux.<sup>4,5</sup> Therefore, anisotropic membrane with dense skin layer on the top become choice of fabrication method as it can exhibit high gas flux and high gas selectivity. There are various factors that are in interplay between air-drying time, concentration of polymer, relative humidity of the surrounding, activity of coagulant bath and many more factors that can influence both the performance and morphology of the membrane.<sup>6</sup>

Ismail et al. (2017) fabricated polysulfone (PSf) membrane at various concentrations and tested their physical properties of the fabricated membrane.<sup>7</sup> Their study found that increased polymer concentration enhanced the tensile strength of the flat sheet (FS) membrane due to the suppression of macrovoids formation at higher polymer concentrations. Moreover, the initiation position for the formation of macrovoids is also affected by the degree of entanglement of the polymer chain. High polymer concentration caused higher polymer chain entanglement thus making the initiation macrovoids formation to be away from the membrane surface and deep in the structure of the membrane. Longer time needed to induce phase separation also will caused the macrovoids initiation to starts from within the membrane instead at the surface.<sup>8</sup> Presence of macrovoids are generally not favourable as it will weaken the mechanical strength of the membrane.<sup>9</sup>

Ahmad et al. (2022) fabricated poly(4-methyl-1-pentene) (PMP) at various concentrations where they found that PMP with 5 wt% concentration are able to form dense membrane with 5.91 GPU of CO<sub>2</sub> permeance with ideal CO<sub>2</sub>/N<sub>2</sub> selectivity of 11.57.<sup>10</sup> When the same concentration is used to cast for anisotropic membrane, the permeance improved by 10 times but the ideal CO<sub>2</sub>/N<sub>2</sub> selectivity reduced by half. Bridge et al. (2022) prepared a defect free PSf asymmetric membrane with Cyrene<sup>TM</sup> as the green solvent to study its potential to replace the usually used aprotic polar toxic solvents in membrane fabrication.<sup>11</sup> With 5 s drying time, the fabricated membrane achieved 46 GPU of CO<sub>2</sub> permeance with

ideal CO<sub>2</sub>/N<sub>2</sub> selectivity of 28.8 at 35°C and 2 bar. The high selectivity achieved is attributed to the presence of volatile tetrahydrofuran (THF) as the co-solvent that evaporate during the dry-phase inversion forming the defectfree skin layer. Haider et al. (2020) prepared asymmetric PES FS membrane with 22 wt% where they achieved 145.4 GPU with ideal CO<sub>2</sub>/N<sub>2</sub> and CO<sub>2</sub>/CH<sub>4</sub> selectivity of 0.982 and 0.66, respectively.<sup>12</sup> When polydimethylsiloxane (PDMS) coating is applied, CO<sub>2</sub> permeance dropped to 19.47 GPU while the ideal CO<sub>2</sub>/N<sub>2</sub> and CO<sub>2</sub>/CH<sub>4</sub> selectivity increased to 2.66 and 1.64, respectively.

Although homogenous dense membrane can be formed at the concentration lower than critical concentration value, the formation of anisotropic membrane at low concentration is not free from defect. Thus, this negatively affect the ideal gas selectivity. Even though the defects can be mitigated by introducing volatile solvents, this will inherently increase the complexity of the thermodynamics of the dope mixture and alter the stability of the dope mixture. This difficulty is more pronounced with mixed matrix membrane fabrication. The role of polymer concentration and its effect onto the morphology and performance of the fabricated membrane using a PES/N-methyl-2-pyrrolidone (NMP) system through simple drywet phase inversion process were demonstrated.

## 2. MATERIAL AND METHODOLOGY

### 2.1 Materials

PES flakes (Ultrason E6020P, MW = 58,000 g/mol) were procured from BASF (Germany) and used to form the membrane. NMP (Purity > 99.5 wt.%) were purchased from Merck (Germany) used as solvent to dissolve the PES polymer flakes. High gas purity cylinder of CO<sub>2</sub>, N<sub>2</sub> and CH<sub>4</sub> were purchased from local company, Alpha Gas Solution Sdn. Bhd. (Malaysia). All chemicals procured were used as received without further purification.

### 2.2 Flat Sheet Membrane Fabrication

FS membranes were fabricated with solvent casting method.<sup>13</sup> Prior to dope formulation, the PES flakes were kept in an oven at 70°C overnight to remove any moisture content that may present in the flakes. The dried PES flakes were weighed and dissolved into NMP solvent under stirring conditions (350 rpm) at 65°C for 24 h to allow complete dissolution of the PES flakes. The PES flakes were added gradually into the NMP solvent to prevent aggregation of polymer particles. For 20 wt% (PES-1) and 25 wt% (PES-2), the dope solution was stirred with magnetic stirrer while for 29.4 wt% (PES-3), 30 wt% (PES-4) and 35 wt% (PES-5), the

dope solution was stirred using mechanical stirrer due to the high viscosity. After mixing overnight, the dope solution was degassed using ultrasound sonicator bath to remove any bubbles formed inside the solution. The degassed dope solution was casted with predetermined thickness of 400  $\mu\text{m}$  at room temperature (25°C) on a glass substrate. The relative humidity was kept within the range of 56% to 60% during the membrane casting process. Thirty seconds after the dope solution casted, the thin film formed on the glass substrate were immersed in distilled water at room temperature overnight to allow complete phase inversion. The membrane formed was then thoroughly washed with distilled water and dried before use in gas permeation experiment. Table 1 shows the summary of the condition for FS membrane casting.

Table 1: Membrane sample ID and condition for FS membrane casting.

Sample ID	Gardner's knife thickness ( $\mu\text{m}$ )	Air-drying time (s)	Room condition	PES/NMP composition (wt%)
PES-1				20/80
PES-2				25/75
PES-3	400	30	25°C RH: 56%–60%	29.4/70.6
PES-4				30/70
PES-5				35/65

\*RH = Relative humidity

### 2.3 Characterisation and Analysis

The viscosity of the dope solutions was measured using viscometer at 25°C. Surface and cross-sectional area of the membranes were observed using scanning electron microscopy (SEM) with tabletop TM3000 (Hitachi Ltd., Tokyo). Prior to cross-sectional area observation, the membranes were immersed in liquid  $\text{N}_2$  and freeze-fractured to prevent deformation of the membrane structure. The surface porosity of the membrane and the cross-section thickness were determined with ImageJ software based on the SEM image. The measurement was taken from three different areas. Measurement of the surface porosity was done by converting the SEM images into Red-Green-Blue (RGB) mode and split into three different “channel” with either Red, Green and Blue colour mode. Essentially, SEM images is in black and white by nature, hence they appear the same regardless of the channel chosen. The chosen image was converted into 8-bit mode to present. Brightness and contrast were adjusted to remove background noise in the chosen image. Automatic thresholding was employed to convert the image into binary (black and white) where the black areas represent the pores while white area represent the surface of the membrane. The percentage area of the black spots

were obtained from the ImageJ software.<sup>14</sup> Fourier transform infrared attenuated total reflectance (FTIR-ATR) (Perkin Elmer, United States) were used to study the chemical bond of the membranes.

## 2.4 Gas Permeation Performance

The single gas permeation performance was done with constant volume–variable pressure method. For FS membrane, a circular-shaped membrane was cut from the FS membrane and embedded into the membrane cell with effective permeation area of 3.14 cm<sup>2</sup>. The module was then attached to the gas permeation test rig. Prior to single gas measurement, the whole rig was vacuumed with a vacuum pump through the upstream purge stream to remove any adsorbed gas or moisture in the rig.<sup>15</sup> Then the rig was flushed with test gas to purge the remaining trace humid air molecules. The permeation experiment was then commenced for pressure ranging from 2 bar to 5 bar. The feed of pure gas was fed in the sequence of N<sub>2</sub>, followed by CH<sub>4</sub> and lastly CO<sub>2</sub>. For each change of feed gas cycle, the gas permeation test rig was vacuumed to remove trace gas molecules and flushed with the test gas. To ensure consistency, each measurement was repeated three times. The reported values are the average of three readings. The equation used to calculate the gas permeance of individual gases and the ideal selectivity are shown by Equation 1 and Equation 2, respectively.

$$\frac{P}{l} = \frac{273.15 \times 10^6 \times V}{760AT \left( \frac{P_o \times 76}{14.696} \right)} \left( \frac{dp}{dt} \right) \quad (1)$$

Where  $P/l$  is the pressure-normalised flux of the gas expressed in GPU [1 GPU =  $1 \times 10^{-6}$  cm<sup>3</sup>·cm/(cm<sup>2</sup>·s·cm Hg)],  $V$  is the volume of gas permeate,  $l$  is the thickness of dense skin layer (cm),  $A$  is the permeation area (cm<sup>2</sup>),  $P_o$  is the upstream pressure (psi) and  $dp/dt$  is the pressure gradient (psia/s). The ideal selectivity of the gas pair can then be calculated using Equation (2):

$$\alpha_{i,j} = \frac{\left( \frac{P}{l} \right)_i}{\left( \frac{P}{l} \right)_j} \quad (2)$$

Where  $\alpha_{i,j}$  is the ideal selectivity of the gas. Ideal gas is defined as the ratio of pure gas pressure-normalised flux ( $P/l$ ) calculated from Equation (1). The subscript  $i$  and  $j$  correspond to the species of the gas tested. Gas permeation test were repeated at least twice, and all the result reported are the averaged value.

### 3. RESULTS AND DISCUSSION

#### 3.1 FTIR-ATR Analysis

FTIR-ATR was used to study the chemical bond presence in the fabricated PES FS membrane. Figure 1 shows the overall spectrum while. The absorption peak at  $1,004\text{ cm}^{-1}$  and  $1,240\text{ cm}^{-1}$  shows the stretching of aromatic ether linkage ( $-\text{C}-\text{O}-\text{C}-$ ) that presence in PES polymer. The absorption peak that appears at  $1,148\text{ cm}^{-1}$  and  $1,296\text{ cm}^{-1}$  is assigned to the stretching caused by symmetric and asymmetric sulfone group of PES while the absorption peak at  $1,484\text{ cm}^{-1}$  and  $1,576\text{ cm}^{-1}$  is assigned to the peak by  $(\text{CH}_3-\text{C}-\text{CH}_3)$  group and  $\text{C}=\text{C}$  aromatic ring respectively. Lastly, the peak  $1,660\text{ cm}^{-1}$  is assigned to the carbonyl group that presence in the PES membrane structure.<sup>16,17</sup> The FTIR-ATR analysis also confirmed that there is no foreign substance or residual solvent in the anisotropic PES membrane following the post treatment by immersion in distilled water for 3 days after membrane fabrication.

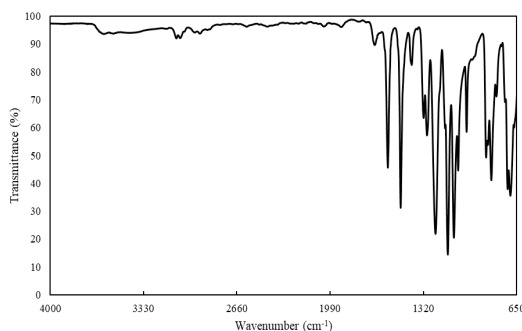


Figure 1: FTIR-ATR spectra of pristine PES membrane.

#### 3.2 Morphology of the Membrane

The viscosity of the dope solution at various PES concentrations are shown in Figure 2. The viscosity shows exponential increase with increasing PES concentration as viscosity is a function of polymer concentration. At higher polymer content, the polymer chain entanglement becomes significant, thus increasing the drag force between the polymer chain attributing to the higher viscosity.<sup>8</sup> The intersection of tangent line between high polymer content and low polymer content is the critical concentration region where the polymer chain entanglement starts to occurs notably.<sup>18</sup>

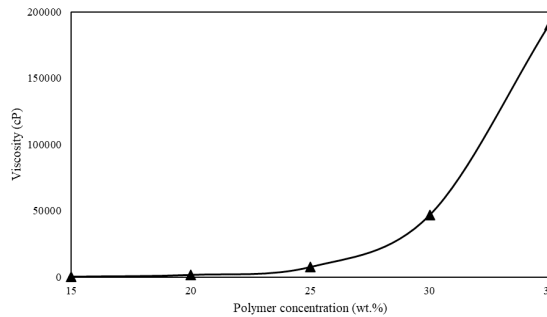
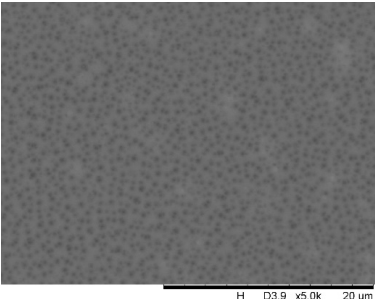
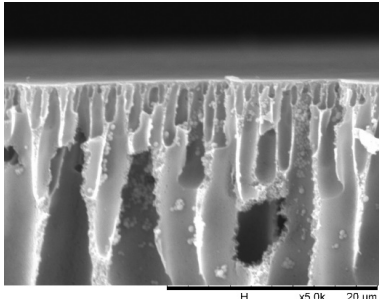
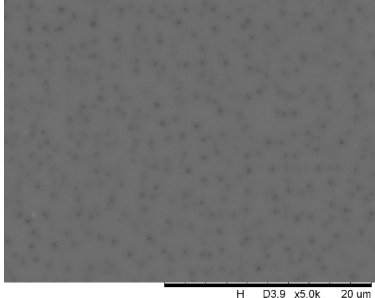
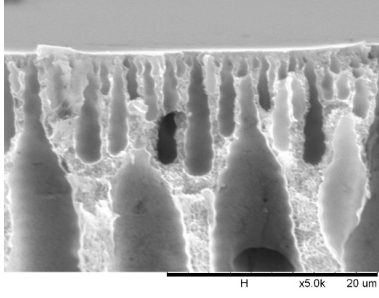
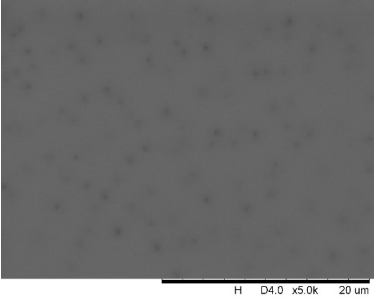
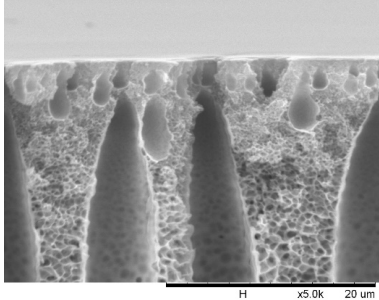


Figure 2: Viscosity against polymer concentration.

The morphology of the membranes is shown in Figure 3. From the surface morphology of the membrane, it can be seen that with increasing concentration, the surface pore virtually disappears until the surface become completely absent of pores at PES-4. For PES-5, the surface appeared to have lines of defect that may arise due to the extremely viscous solution during solution casting, thus exerting excessive shear on the surface of the membrane and difficulties in spreading it evenly in the casting direction. The surface porosity of PES-1 is 36.95% and reduced by almost two times for PES-2. The surface porosity becomes very close to 0 when the concentration is further. Virtually, the formation of pinholes on the membrane surface becomes lesser at higher PES concentration. The observation is similar as observed by Ahmad et al. (2017).<sup>19</sup> For gas separation membrane, the presence of the pores are generally not favourable as it will adversely affect the gas separation performance.<sup>20</sup> The presence of pores on the surface of the membrane enhance CO<sub>2</sub> permeance, however it is also accompanied by reduced CO<sub>2</sub>/N<sub>2</sub> and CO<sub>2</sub>/CH<sub>4</sub> ideal selectivity as the pores are too big, hence no separation occurs at the skin layer of the membrane. Therefore, dense surface is more favourable for gas separation membrane as the separation is generally governed by solution-diffusion mechanism.

The cross-sectional morphology of the membrane from Figure 3 shows the membrane exhibit finger-like projection at low PES concentration and slowly disappear with increasing concentration. When the PES concentration is increased further to 25 wt%, the skin layer appears to be more visible on the top part of the membrane and become more apparent once the PES concentration pass the critical concentration. A distinctive skin layer can be seen for PES-5. Furthermore, the finger-like projection is also suppressed when the concentration of the PES increases. The phenomena could be ascribed to the retarded phase inversion process with increased polymer concentration due to the high entanglement of polymer chain leading to high viscosity of the dope solution.<sup>8</sup> High polymer

concentration increase the solubility differences between solvent and coagulant leading to weaker interaction between solvent and non-solvent, thus the demixing rate becomes slower reducing the finger-like projection across the cross section of the membrane and encourage formation of big polymer aggregate.<sup>21</sup> With increased skin layer thickness, the membrane will impose greater resistance to the gas penetrant hence reducing the flux of the penetrating gas. Additionally, the overall thickness of the membrane increase with increasing polymer content which is also ascribed to the increasing viscosity of the dope solution.<sup>22</sup> The surface porosity and overall thickness of the membranes are presented in Table 2.

Membrane sample	Surface	Magnified cross-section
PES-1		
PES-2		
PES-3		

(continued on next page)

Figure 3 (continued)

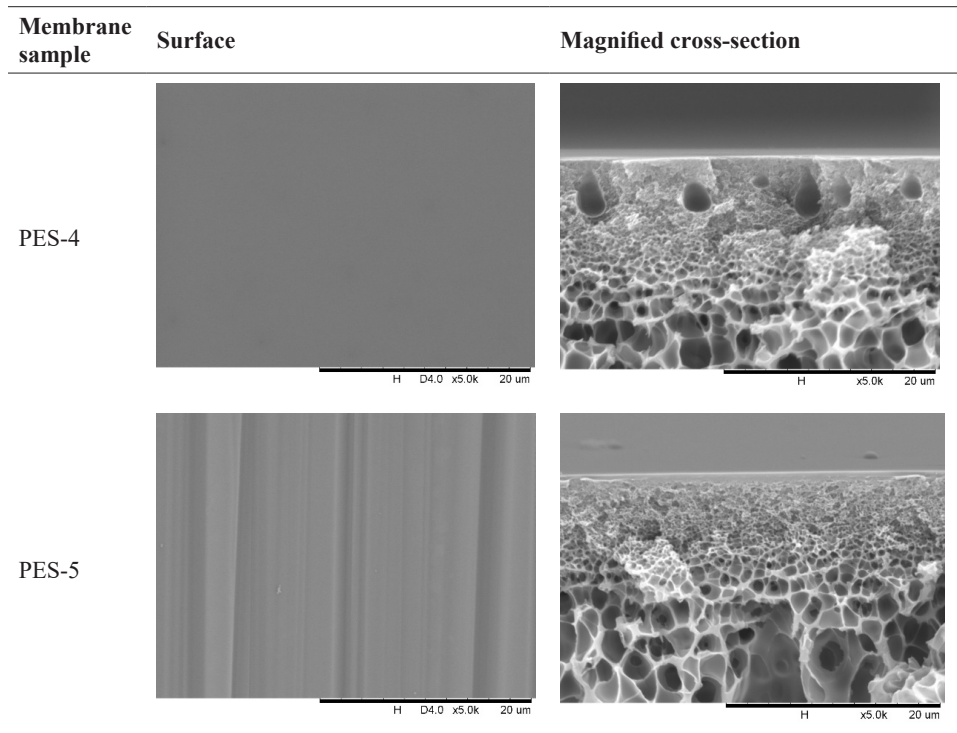


Figure 3: Surface and cross-sectional morphology of the PES FS membranes.

Table 2: Surface porosity and thickness of the membrane.

Membrane sample	Thickness ( $\mu\text{m}$ )	Surface porosity (%)
PES-1	201.5	36.949
PES-2	213	13.785
PES-3	214	3.406
PES-4	230	0.070
PES-5	1040	~0

PES FS membranes were tested at various pressure and the result is presented in Figure 4. Pure  $\text{CO}_2$  gas permeance drops with increasing PES dope concentration of the casted solution. At 20 wt% of PES,  $\text{CO}_2$  permeance is recorded to be the highest which is 154.9 GPU at 2 bar among other PES concentration.  $\text{CO}_2$  permeance reduce in an exponential trend when the PES concentration is further increased up to 35 wt%. Additionally, the  $\text{CO}_2$  permeance increase in linear fashion with increasing upstream pressure due to the pressure difference across the membrane.

The trend can be observed for all of the PES FS membranes. The decreasing trend of CO<sub>2</sub> permeance is accompanied by increased trend of CO<sub>2</sub>/N<sub>2</sub> and CO<sub>2</sub>/CH<sub>4</sub> ideal selectivity. For 20 wt%, the ideal selectivity of CO<sub>2</sub>/N<sub>2</sub> and CO<sub>2</sub>/CH<sub>4</sub> is lower than 1 and close to the value of Knudsen's selectivity. This indicates the gas diffusion through the membrane is governed by Knudsen's diffusion due to significant presence of pores.<sup>23</sup> When PES concentration is increased to 25 wt%, the ideal selectivity of both CO<sub>2</sub>/N<sub>2</sub> and CO<sub>2</sub>/CH<sub>4</sub> is very close; one revealing that the gas diffusion is governed by Poiseuille's flow where the existing pore is too big to discriminate the gas penetrant by size exclusion. Hence, all gas species can pass through the membrane at the same rate. However, when PES concentration is increased to 30 wt%, the ideal selectivity of CO<sub>2</sub>/N<sub>2</sub> and CO<sub>2</sub>/CH<sub>4</sub> increased to 6.26 and 4.03, respectively, and exponentially increased at PES concentration of 35 wt%. The increased in ideal selectivity of the gases indicates that there is formation of skin layer forming on the surface of the membrane, thus capable discriminating the gas by solution-diffusion mechanism.<sup>18</sup> Although, it can be said that the dense skin layer formed are defective since the ideal selectivity factor is < 80% of the intrinsic value.<sup>24</sup> The observation is consistent with the morphology of the membrane as observed by SEM image as presented in Figure 2. Meanwhile with increased pressure, there is no drastic changes in the selectivity observed as the gases experience similar increment of flux with increasing upstream pressure.<sup>25</sup> The critical concentration of PES of 29.4 wt% were tested and showed ideal selectivity of greater than 1. The ideal selectivity of CO<sub>2</sub>/N<sub>2</sub> and CO<sub>2</sub>/CH<sub>4</sub> are 2.03 and 1.48, respectively at 2 bar. This indicates that the critical concentration is sufficient to ensure formation of dense skin layer to allow the gas to be separated, albeit the surface is defective. For defective skin layer, the gas transport mechanism is not only by solution-diffusion alone but the combination of solution-diffusion, Knudsen's diffusion and Poiseuille's flow mechanism.<sup>26</sup> The defective surface layer could be ascribed to the membrane being subjected to fast demixing process during the fabrication process, thus leading to incomplete coalescence of polymer with pinholes.<sup>27</sup> Increasing the PES concentration beyond the critical concentration would be counter intuitive since the flux will be severely reduced despite of the high ideal selectivity. The balance between CO<sub>2</sub> permeance and ideal selectivity is sufficiently catered by utilising the critical concentration of the polymer solution. To cover the defective skin layer, PDMS coating is usually applied to the surface of the membrane to bring back the intrinsic separation properties of the anisotropic membrane.<sup>28</sup>

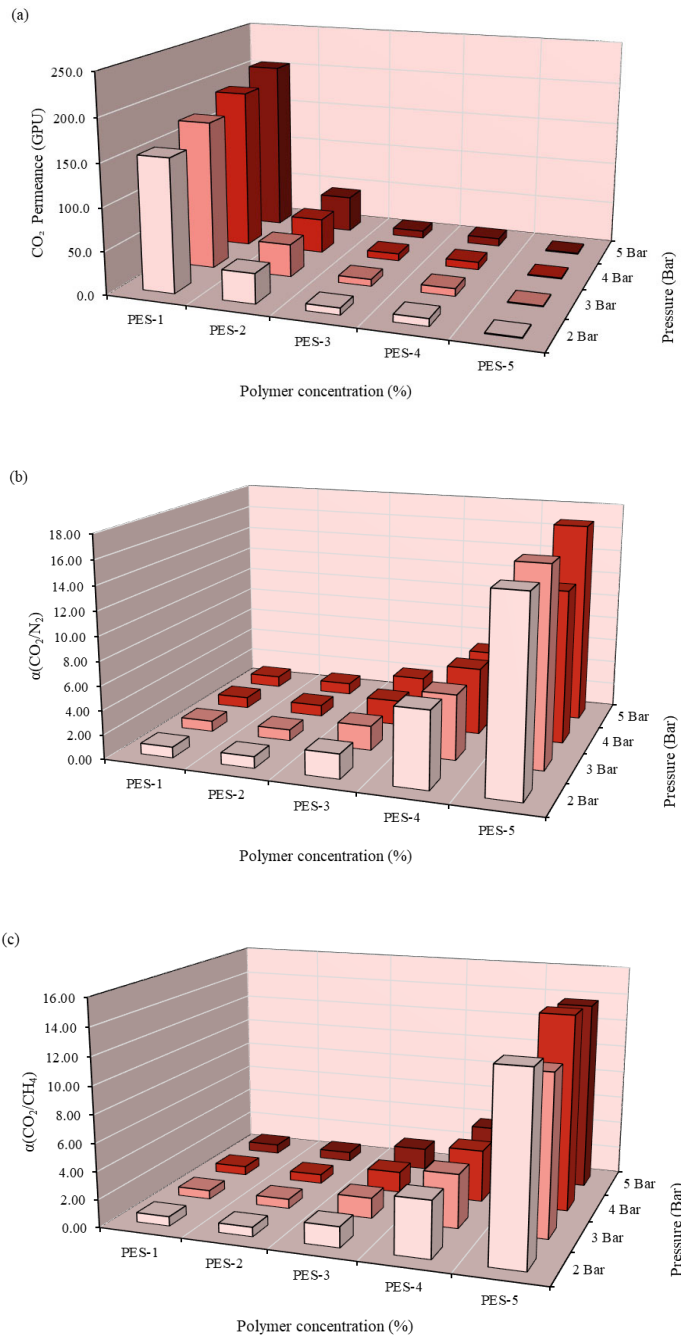


Figure 4: Gas separation performance of FS membrane (a)  $\text{CO}_2$  permeance, (b)  $\text{CO}_2/\text{N}_2$  ideal selectivity and (c)  $\text{CO}_2/\text{CH}_4$  ideal selectivity.

#### 4. CONCLUSION

From this study, PES membrane for gas separation is successfully fabricated with various concentration. It is shown that the polymer concentration plays a critical role in the formation of selective skin layer of the membrane to allow gas separation to occur. Moreover, the elongated finger-like structure become less obvious across the membrane with increased PES concentration while the thickness of the membrane increased with increasing polymer concentration. The gas flux is high at lower polymer concentration accompanied by low CO<sub>2</sub>/N<sub>2</sub> and CO<sub>2</sub>/CH<sub>4</sub> ideal selectivity while the trend is reversed once the PES concentration exceeds the critical concentration. The critical concentration of PES/NMP system is determined to be 29.4 wt% in this study where at the pressure of 2 bar, the CO<sub>2</sub> permeance, CO<sub>2</sub>/N<sub>2</sub> and CO<sub>2</sub>/CH<sub>4</sub> are 8.1 GPU, 2.03 and 1.48, respectively.

#### 5. ACKNOWLEDGEMENTS

The authors acknowledged the financial assistance and facilities provided by Universiti Sains Malaysia and Fundamental Research Grant Scheme by Ministry of Higher Education Malaysia (FRGS/1/2020/TK0/USM/01/4).

#### 6. REFERENCES

1. Wang, X. & Song, C. (2020). Carbon capture from flue gas and the atmosphere: A perspective. *Front. Energy Res.*, 8. <https://doi.org/10.3389/fenrg.2020.560849>
2. Zainuddin, M. I. F. & Ahmad, A. L. (2022). Mixed matrix membrane development progress and prospect of using 2D nanosheet filler for CO<sub>2</sub> separation and capture. *J. CO<sub>2</sub> Util.*, 62, 102094. <https://doi.org/10.1016/j.jcou.2022.102094>
3. Dharupaneedi, S. P. et al., (2019). Membrane-based separation of potential emerging pollutants. *Sep. Purif. Technol.*, 210, 850–866. <https://doi.org/10.1016/j.seppur.2018.09.003>
4. Henis, J. M. S. & Tripodi, M. K. (1981). Composite hollow fiber membranes for gas separation: The resistance model approach. *J. Memb. Sci.*, 8(3), 233–246. [https://doi.org/10.1016/S0376-7388\(00\)82312-1](https://doi.org/10.1016/S0376-7388(00)82312-1)
5. Henis, J. M. S. & Tripodi, M. K. (1983). The developing technology of gas separating membranes. *Sci.*, 220(4592), 11–17. <https://doi.org/10.1126/science.220.4592.11>
6. Ahmad, A. L. et al. (2019). Hollow fiber (HF) membrane fabrication: A review on the effects of solution spinning conditions on morphology and performance. *J. Ind. Eng. Chem.*, 70, 35–50. <https://doi.org/10.1016/j.jiec.2018.10.005>
7. Ismail, N. M. et al., (2017). Effect of polymer concentration on the morphology and mechanical properties of asymmetric polysulfone (PSf) membrane. *J. Appl. Mem. Sci. Technol.*, 21(1), 33–41. <https://doi.org/10.11113/amst.v21i1.107>

8. Hung, W.-L. et al. (2016). On the initiation of macrovoids in polymeric membranes – effect of polymer chain entanglement. *J. Membr. Sci.*, 505, 70–81. <https://doi.org/10.1016/j.memsci.2016.01.021>
9. Alibakhshi, S. et al. (2020). Significance of thermodynamics and rheological characteristics of dope solutions on the morphological evolution of polyethersulfone ultrafiltration membranes. *Polym. Eng. Sci.*, 61(3), 742–753. <https://doi.org/10.1002/pen.25613>
10. Ahmad, A. L. et al. (2022). Poly(4-methyl-1-pentene) membrane for CO<sub>2</sub> separation: Performance comparison of dense and anisotropic membrane. *Arab. J. Sci. and Eng.*, 48(7), 8325–8338. <https://doi.org/10.1007/s13369-022-06698-5>
11. Bridge, A. T. et al. (2022). Preparation of defect-free asymmetric gas separation membranes with dihydrolevoglucosenone (Cyrene™) as a greener polar aprotic solvent. *J. Membr. Sci.*, 644, 120173. <https://doi.org/10.1016/j.memsci.2021.120173>
12. Haider, B. et al. (2020). Highly permeable novel PDMS coated asymmetric polyethersulfone membranes loaded with SAPO-34 zeolite for carbon dioxide separation. *Sep. Purif. Technol.*, 248, 116899. <https://doi.org/10.1016/j.seppur.2020.116899>
13. Ahmad, A. L. et al. (2017). Thickness effect on the morphology and permeability of CO<sub>2</sub>/N<sub>2</sub> gases in asymmetric polyetherimide membrane. *J. Phys. Sci.*, 28(1), 201–213. <https://doi.org/10.21315/jps2017.28.s1.13>
14. Xiao, M. et al. (2022). Characterizing surface porosity of porous membranes via contact angle measurements. *J. Membr. Sci. Lett.*, 2(1), 100022. <https://doi.org/10.1016/j.memlet.2022.100022>
15. Ding, S. H. et al. (2023). Nucleophilic substituted NH<sub>2</sub>-MIL-125 (Ti)/polyvinylidene fluoride hollow fiber mixed matrix membranes for CO<sub>2</sub>/CH<sub>4</sub> separation and CO<sub>2</sub> permeation prediction via theoretical models. *J. Membr. Sci.*, 681, 121746. <https://doi.org/10.1016/j.memsci.2023.121746>
16. Madaeni, S. S. et al. (2013). Effect of coating method on gas separation by PDMS/PES membrane. *Polym. Eng. Sci.*, 53(9), 1878–1885. <https://doi.org/10.1002/pen.23456>
17. Yousef, S. et al. (2021). CO<sub>2</sub>/CH<sub>4</sub>, CO<sub>2</sub>/N<sub>2</sub> and CO<sub>2</sub>/H<sub>2</sub> selectivity performance of PES membranes under high pressure and temperature for biogas upgrading systems. *Environ. Technol. Innov.*, 21, 101339. <https://doi.org/10.1016/j.eti.2020.101339>
18. Shamsabadi, A. A. et al. (2013). Role of critical concentration of PEI in NMP solutions on gas permeation characteristics of PEI gas separation membranes. *J. Ind. Eng. Chem.*, 19(2), 677–685. <https://doi.org/10.1016/j.jiec.2012.10.006>
19. Ahmad, A. L. et al. (2017). Synthesis of asymmetric polyetherimide membrane for CO<sub>2</sub>/N<sub>2</sub> separation. *IOP Conf. Ser. Mater. Sci. Eng.*, 206, 012068. <https://doi.org/10.1088/1757-899X/206/1/012068>
20. Choi, S.-H. et al. (2010). Effect of the preparation conditions on the formation of asymmetric poly(vinylidene fluoride) hollow fibre membranes with a dense skin. *Eur. Polym. J.*, 46(8), 1713–1725. <https://doi.org/10.1016/j.eurpolymj.2010.06.001>

21. Ismail, A. F. & Lai, P. Y. (2003). Effects of phase inversion and rheological factors on formation of defect-free and ultrathin-skinned polysulfone membranes for gas separation. *Sep. Purif. Technol.*, 33(2), 127–143. [https://doi.org/10.1016/S1383-5866\(02\)00201-0](https://doi.org/10.1016/S1383-5866(02)00201-0)
22. Torrestiana-Sanchez, B. et al. (1999). Effect of nonsolvents on properties of spinning solutions and polyethers. *J. Membr. Sci.*, 152(1), 19–28. [https://doi.org/10.1016/S0376-7388\(98\)00172-0](https://doi.org/10.1016/S0376-7388(98)00172-0)
23. Madaeni, S. S. et al. (2012). Effect of titanium dioxide nanoparticles on polydimethylsiloxane/polyethersulfone composite membranes for gas separation. *Polym. Eng. Sci.*, 52(12), 2664–2674. <https://doi.org/10.1002/pen.23223>
24. Pesek, S. C. & Koros, W. J. (1994). Aqueous quenched asymmetric polysulfone hollow fibers prepared by dry wet phase separation. *J. Membr. Sci.*, 88(1), 1–19. [https://doi.org/10.1016/0376-7388\(93\)E0150-I](https://doi.org/10.1016/0376-7388(93)E0150-I)
25. Zainuddin, M. I. F. & Ahmad, A. L. (2022). Impact of dope extrusion rate and multilayer polydimethylsiloxane coating on asymmetric polyethersulfone hollow fiber membrane for CO<sub>2</sub>/N<sub>2</sub> and CO<sub>2</sub>/CH<sub>4</sub> separation. *Asia Pac. J. Chem. Eng.*, 17(6), e2829. <https://doi.org/10.1002/apj.2829>
26. Wang, R. & Chung, T. S. (2001). Determination of pore sizes and surface porosity and the effect of shear stress within a spinneret on asymmetric hollow fiber membranes. *J. Membr. Sci.*, 188(1), 29–37. [https://doi.org/10.1016/S0376-7388\(01\)00370-2](https://doi.org/10.1016/S0376-7388(01)00370-2)
27. Ismail, A. F. & Yean, L. P. (2003). Review on the development of defect-free and ultrathin-skinned asymmetric membranes for gas separation through manipulation of phase inversion and rheological factors. *J. Appl. Polym. Sci.*, 88(2), 442–451. <https://doi.org/10.1002/app.11744>
28. Hu, C.-C. et al. (2022). Carbon dioxide enrichment of PDMS/PSf composite membranes for solving the greenhouse effect and food crisis. *J. CO<sub>2</sub> Util.*, 61, 102011. <https://doi.org/10.1016/j.jcou.2022.102011>